Ocean Dynamics (2014) 64:79–88
DOI 10.1007/s10236-013-0674-5

Observations on the flow structures and transport in a simulated warm-core ring in the Gulf of Mexico

Doug Lipinski · Kamran Mohseni

Received: 16 September 2013 / Accepted: 22 November 2013 / Published online: 27 December 2013

Abstract This study presents several new observations from the study of a numerically simulated warm-core ring (WCR) in the Gulf of Mexico based on the ECCO2 global ocean simulation. Using Lagrangian coherent structures (LCS) techniques to investigate this flow reveals a pattern of transversely intersecting LCS in the mixed layer of the WCR which experiences consistent stretching behavior over a large region of space and time. A detailed analysis of this flow region leads to an analytical model of the velocity field which captures the essential elements that generate the transversely intersecting LCS. The model parameters are determined from the simulated WCR and the resulting LCS show excellent agreement with those observed in the WCR. The three-dimensional transport behavior that creates these structures relies on the small radial outflow that is present in the mixed layer and is not seen below the pycnocline, leading to a sharp change in the character of the LCS at the bottom of the mixed layer. The flow behavior revealed by the LCS limits fluid exchange between the WCR and the surrounding ocean, contributing to the long life of WCRs. Further study of these structures and their associated transport behavior may lead to further insights into the development and persistence of such geophysical vortices as well as their transport behavior.

Keywords Ocean · Warm-core ring · Lagrangian · Coherent structures · Transport · Mixing

Responsible Editor: Tal Ezer

D. Lipinski
Institute for Networked Autonomous Systems,
Department of Mechanical and Aerospace Engineering,
University of Florida, Gainesville, FL 32611, USA

K. Mohseni (✉)
Department of Mechanical and Aerospace Engineering,
Institute for Networked Autonomous Systems,
University of Florida, Gainesville, FL, USA
e-mail: mohseni@ufl.edu

K. Mohseni
Department of Electrical and Computer Engineering,
Institute for Networked Autonomous Systems,
University of Florida, Gainesville, FL, USA

1 Introduction

Despite the importance and prevalence of warm-core rings (WCRs) in the Gulf of Mexico (GoM) and other ocean basins, many of the details of the transport and small-scale coherent structures in these flows remain poorly understood. WCRs have a significant impact on oceanic transport and energy balances (Elliott 1979; Lewis et al. 1989; Oey 2008) and can also influence weather patterns including hurricanes due to their interaction with the atmosphere. It is known that hurricanes may rapidly intensify when passing over a WCR (Hong et al. 2000; Shay et al. 2000; Scharroo et al. 2005). Additionally, the mixing behavior in a WCR differs significantly from that of the surrounding ocean and may greatly influence biological activity such as plankton blooms (Franks et al. 1986; Biggs 1992).

The primary purpose of this paper is to present some newly observed structures and their associated transport behavior in a numerically simulated warm-core ring in the Gulf of Mexico. The ring studied here is present in the publicly available ECCO2 global ocean simulation. We have chosen to focus on newly observed small-scale coherent structures seen in the near-surface region (that is, the ocean-atmosphere boundary) of the WCR. To study the structures in these flows, we use the technique of Lagrangian coherent

structures (LCS). This technique is used to identify structures relevant to the Lagrangian transport of fluid. These structures represent barriers to transport and often reveal flow behavior that may be difficult or impossible to detect with Eulerian measures.

In Section 2, we briefly present an overview of the LCS technique before applying this technique to computing the three-dimensional LCS present in numerical simulations of a WCR. In Section 3, the results of these LCS computations are discussed, revealing a previously unobserved type of structure in the mixed layer. Due to the transversely intersecting LCS that appear in this region, we will refer to these structures as "checkerboard LCS." The Lagrangian flow behavior in the checkerboard LCS region is also investigated in Section 3. In Section 4, a simple analytical model is presented which produces similar LCS structures and provides several insights into the mechanisms through which these structures are generated. Finally, we conclude with a brief discussion of the results and possible avenues for new research.

2 Lagrangian coherent structures

The term LCS has come to refer to a class of techniques used to identify coherent structures in aperiodic, finite time flows. In steady state or periodic systems, classical dynamical systems techniques can be used to identify hyperbolic fixed points and their stable and unstable manifolds as well as other invariant manifolds in the system. These structures may then be used to study the flow topology and the corresponding mixing and transport in the system. However, in systems with general time dependence, the same techniques no longer apply. To address this shortcoming and identify coherent structures in systems with general time dependence, various methods have been proposed. One of the most popular and successful methods has been the use of the finite time Lyapunov exponent (FTLE) to identify regions of locally maximum stretching in the flow (Haller and Yuan 2000; Shadden et al. 2005). Intuitively, one expects that regions with qualitatively different dynamics will be separated by a thin region of very large Lagrangian stretching (Haller and Yuan 2000). Fluid parcels that straddle the boundary between two regions will be greatly deformed and stretched over time as they separate into different regions.

The notion of defining coherent structures by the stretching at their boundaries was formalized in Shadden et al. (2005) by defining LCS as ridges in the FTLE field. This method of defining and computing LCS has since proven to be very effective in many cases, but it is worth noting that there are alternative definitions as well. In particular, Haller and others have developed a variational formulation for computing LCS (Haller 2011; Farazmand and Haller 2012), there are methods for finding "distinguished" trajectories (Ide et al. 2002; Madrid and Mancho 2009), and there are methods for finding maximally invariant sets (Dellnitz et al. 2005; Froyland and Padberg 2009). In this paper, we will use LCS as defined in Shadden et al. (2005): ridges of the FTLE field.

LCS techniques are primarily useful for determining and examining the Lagrangian transport of a system. In the past, these techniques have been used to investigate unsteady separation (Haller 2004) and the flow over an airfoil (Cardwell and Mohseni 2008), transport in jellyfish swimming and feeding (Lipinski and Mohseni 2009; Peng and Dabiri 2009), three-dimensional turbulence (Green et al. 2007), atmospheric transport (Lekien and Ross 2010), and many other applications. LCS provide a way to precisely identify the extent or boundaries of coherent structures and, correspondingly, a way to quantify their impact on transport phenomena. Crucially, LCS identify *barriers to transport* and therefore reveal the structure underlying mixing and transport in a flow.

LCS have been applied to many ocean flows with good results. LCS have been used to study optimal pollution mitigation (Coulliette et al. 2007), transport in a wind-driven double gyre (Coulliette and Wiggins 2001), identify mesoscale eddies (Beron-Vera et al. 2008), and even investigate the transport of oil from the Deepwater Horizon oil spill (Mezić et al. 2010 Huntley et al. 2013; Olascoaga and Haller 2012). Most ocean studies using LCS have focused solely on surface flows and used two-dimensional LCS computations. The expectation has been that since oceanic flows are highly stratified and vertical velocities are typically orders of magnitude smaller than the horizontal velocities, two-dimensional computations are appropriate. However, the length scales in the vertical direction are also orders of magnitude smaller than those in the horizontal, leading to flow gradients in the vertical direction that may exceed those in the horizontal. Recently, researchers have begun to focus more directly on the impacts of three-dimensionality on ocean LCS, noting that three-dimensional effects may be critically important even if the vertical velocity component is small (Sulman et al. 2013).

To compute the LCS, it is necessary to first compute the FTLE field. The most common method for doing so involves seeding a region of the flow with a grid of passive drifter particles at some initial time t_0 and advecting these particles with the flow field for some integration time T. This gives an approximation to the flow map

$$\mathbf{\Phi}_{t_0}^{T}(\mathbf{x}_0) = \mathbf{x}_0 + \int_{t_0}^{t_0+T} \mathbf{v}(\mathbf{x}(t), t)dt. \tag{1}$$

Once the flow map has been computed, the Cauchy-Green deformation tensor is computed as

$$\Delta = \left(\frac{d\mathbf{\Phi}}{d\mathbf{x}_0}\right)^* \left(\frac{d\mathbf{\Phi}}{d\mathbf{x}_0}\right), \tag{2}$$

where * denotes the transpose operator. This tensor contains information about the geometric deformation of the flow. The FTLE is then given by

$$\sigma_{t_0}^T(\mathbf{x}_0) = \frac{1}{|T|} \ln \sqrt{\lambda_{\max}}, \tag{3}$$

where $\lambda_{\max}$ is the maximum eigenvalue of Δ. Note that the integration time T may be either positive or negative so for any flow, there are always two sets of LCS. For $T > 0$, the LCS are typically repelling structures, and for $T < 0$, they are attracting. Additionally, the magnitude of T should be chosen so that sufficient detail is resolved in the LCS. As T is increased, more LCS are revealed, but if T is too large, the complexity of the resulting structures may be difficult to interpret.

Once the FTLE field has been computed, the LCS are often visualized by directly plotting the FTLE field. The LCS are defined as ridges in the FTLE field which are visible just as ridges are visible on a topographical map. Various mathematical definitions of ridges are available but this choice does not seem to greatly affect the resulting LCS. For well-defined ridges, the LCS typically permit very low or negligible flux and can be thought of as denoting barriers to fluid transport (Shadden et al. 2005). If desired, one may explicitly extract the ridges from the FTLE field in an additional step to obtain the LCS.

In this study, we have used an efficient ridge tracing algorithm to directly compute the LCS ridge surfaces in the WCR. This method greatly speeds the LCS computations by detecting some initial points on the LCS ridges and then tracing the ridges through space. By avoiding computations away from the FTLE ridges, the algorithm reduces the computational complexity from $\mathcal{O}(\delta x^{-3})$ to $\mathcal{O}(\delta x^{-2})$ in three-dimensional domains (Lipinski and Mohseni 2012). Additionally, we have verified that all results presented below are insensitive to grid refinement. Combined with the good agreement between the observations presented in Section 3 and the analytical model of Section 4, this gives a high level of confidence that the results are not due to numerical artifacts.

3 Observations from a simulated WCR

The observations presented here are based on data from the cube92 run of the ECCO2 global ocean simulation which is publicly available at http://ecco2.jpl.nasa.gov/. All results discussing the WCR refer to the output of this numerical simulation, not to physical measurements of a real-world WCR. However, there is significant evidence that the ECCO2 model captures many aspects of the real ocean on this scale and generates realistic eddies and near-surface ocean dynamics.

The ECCO2 model is an eddy-resolving finite volume simulation that uses a cube–sphere grid projection with an average spacing of 18 km in the horizontal and 50 vertical levels with spacing ranging from 10 m near the surface to about 450 m at a maximum depth of 6,150 m. The data is saved as 3-day averages on a quarter degree latitude-longitude grid with 50 vertical levels. The underlying model is the MIT general circulation model (MITgcm, Marshall et al. 1997). The model is a forward run simulation using optimized values of uncertain parameters (such as bottom drag) which are calculated by minimizing the misfit between data and simulation using the Green functions technique. This results in a realistic and dynamically/physically consistent model. However, because the model is forward run without data assimilation, it should not be expected to closely align with the precise state of the real ocean at any particular later time. The model includes accurate bathymetry and is coupled to a sea-ice model for accurate simulation of the polar oceans. Atmospheric forcing uses the NCEP-NCAR reanalysis (Kanamitsu et al. 2002). For additional details of the ECCO2 model, see Menemenlis et al. (2008).

There are some unknown factors with regards to the accuracy of the model, including the level of accuracy of the vertical velocity components. However, the vertical velocities in the WCR appear in line with previously published results (Flierl and Mied 1985; Franks et al. 1986; Kishi 1994) and the LCS techniques used in this paper are relatively insensitive to small errors in the velocity field (Haller 2002). As will be seen in Section 4, the checkerboard LCS structures observed below do not require a nonzero vertical velocity component. Furthermore, several past studies have used the ECCO2 model output to investigate eddy processes, finding results that support the utility of the simulation (Volkov and Fu 2008; Volkov et al. 2008; Fu 2009; Chen 2013). In particular, Fu (2009) found good agreement between observations from satellite altimetry data and eddy propagation in the ECCO2 model, suggesting that the model accurately captures eddy propagation and the surface behavior of ocean eddies.

We focus on the structure and transport of a warm-core ring in the Gulf of Mexico as found in the ECCO2 simulation on 1 February 2010. WCRs periodically form in the GoM when the loop current in the eastern GoM pinches off in a closed ring which contains warm Caribbean water. These rings typically persist for about 7–13 months (Sturges and Leben 2000) as they drift slowly across the GoM before dissipating in the western GoM (Hurlburt and Thompson 1980).

In WCRs, the flow field is largely two-dimensional, with horizontal flow speeds on the order of 1 m s^{-1} and vertical speeds three to four orders of magnitude smaller. These vertical flow speeds observed in the WCR from the ECCO2 model are roughly in line with those seen in past studies (Flierl and Mied 1985; Franks et al. 1986; Kishi 1994). However, the horizontal length scales are on the order of 100 km while the vertical lengths scales are a few hundred meters. In combination, this means that flow gradients in the vertical direction may be of the same order or larger than those in the horizontal direction. Because of this, even a small vertical displacement may have a large impact on the trajectories of fluid particles and the full three-dimensional flow structure must be considered when analyzing fluid transport in WCRs.

A view of the near-surface LCS in the GoM on 1 February 2010 is shown in Fig. 1. We have computed the three-dimensional LCS in the GoM using a ridge tracking algorithm to speed computations (Lipinski and Mohseni 2012). An integration time of $T = \pm 4$ weeks was used. This time was chosen to reveal the major structures in the flow. In Fig. 1, the loop current is clearly visible in the eastern GoM as it enters through the Yucatan Channel and exits through the Florida Straits. A recently shed WCR is in the central GoM and an older WCR is visible in the western GoM. Below, we will focus on the single WCR in the central GoM.

Figure 2 shows a vertical cross section of the LCS in this WCR. There are several features of note in this figure. First, the LCS reveal a closed bottom to the WCR. In this part of the WCR, the attracting and repelling LCS are nearly parallel and prevent transport in or out of the eddy. The LCS

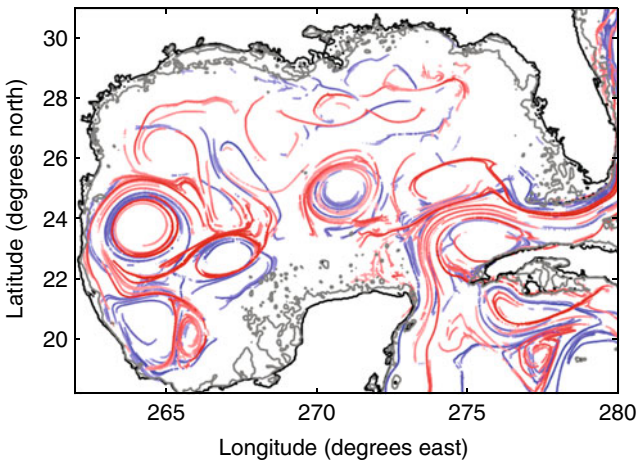

Fig. 1 A two-dimensional slice of the near-surface LCS in the Gulf of Mexico as computed from the ECCO2 dataset for 1 February 2010. Attracting LCS are shown in *red* and repelling are shown in *blue*. A large WCR is present in the center of the GoM and an older ring is in the western GoM. The loop current is also clearly visible

in this region are relatively simple and the primary transport within the WCR near these structures is simply azimuthal flow around the WCR as expected. These LCS denote the separation between fluid that recirculates in the WCR and that which passes by outside: the Lagrangian boundary to the WCR. The source of the stretching giving rise to these LCS is the divergence of trajectories inside and outside the WCR. The clear LCS in this region indicate limited transport into or out of the eddy at depth which is likely one of the reasons WCRs persist for so long. Additionally, this closed bottom indicates that the WCR has limited influence below a certain depth (about 550 m in this case) and fluid below this depth does not get entrained or carried with the WCR. The closed bottom and finite depth of the WCR potentially allows for volumetric computations to determine precisely how much water is carried with the WCR and quantify the corresponding influence on heat, salt, and mass balances in the GoM.

Next, we note a clear difference between the LCS below about 120 m and those above with a sharp transition between these two regions. This 120-m depth marks the bottom of the mixed layer in the WCR. Below this depth, the attracting (red) and repelling (blue) LCS are approximately aligned with one another. However, in the mixed layer, the attracting and repelling LCS intersect transversely, forming a cross-hatched or "checkerboard" pattern. This checkerboard pattern is a new flow structure which has not been previously reported in geophysical flows. The dynamical impacts and underlying flow structure of the checkerboard LCS are not immediately obvious, and likely arise through more complex behavior than the transport that causes the parallel LCS that appear below the mixed layer.

To investigate the flow behavior within the checkerboard region, we place a box of passive drifter particles in this region of the WCR and track their motion over time. The particle positions are shown after 0, 12.5, and 25 days in Fig. 3. The box is initially ≈21 km across in the latitudinal and longitudinal directions and covers a depth range of 50 m. As can be clearly seen in Fig. 3, the initial box of drifter particles is quickly stretched and wrapped around the circumference of the WCR while being compressed in the radial direction. The box very quickly becomes greatly deformed by the horizontal velocities in the flow, but very little motion occurs in the vertical direction. Although it is difficult to see in Fig. 3, the box is also slowly compressed in the vertical direction and pushed upwards while being sheared in the radial direction with particles near the surface moving radially outward with respect to those below. The compression and upward motion is a small effect compared to the other motions observed. The near-surface radial outflow is expected due to friction-based disruption of the cyclo-geostrophic balance that is present in much of the WCR.

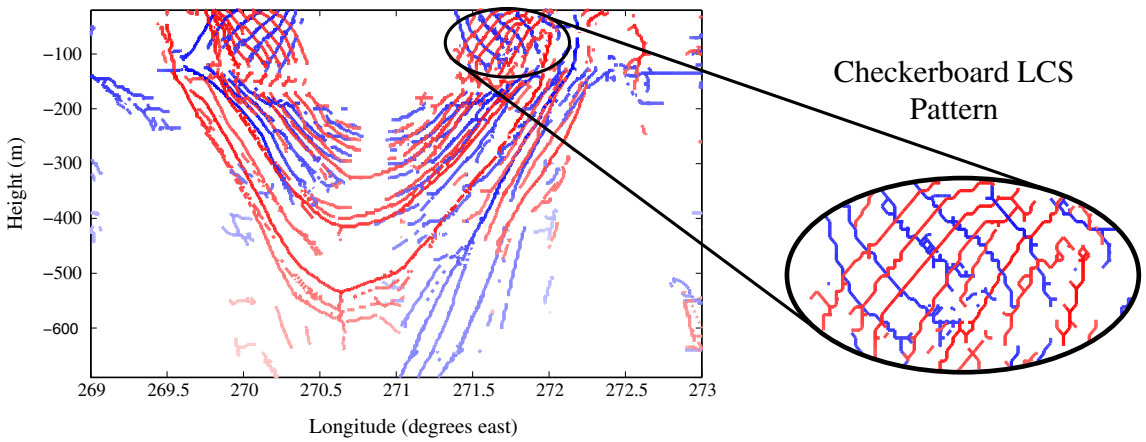

Fig. 2 A vertical cross section of the LCS in a warm-core ring in the Gulf of Mexico computed from the publicly available ECCO2 dataset. The *inset* shows the characteristic "checkerboard" pattern formed by the interaction of the attracting (*red*) and repelling (*blue*) LCS

This last point merits some additional explanation since the radial outflow will be a critical component of the analytical flow presented in Section 4. A near-surface radial outflow has been previously observed in measurements of the near-surface velocity structure of a WCR (Joyce and Kennelly 1985; Olson et al. 1985) as well as numerical models (Flierl and Mied 1985). This result should be expected given the near-surface structure of the WCR, frictional effects, and the specifics of the cyclo-geostrophic balance. The cyclo-geostrophic balance in a WCR is described by the equation

$$|fv| = \left|\frac{v^2}{r}\right| + \left|\frac{1}{\rho}\frac{\partial p}{\partial r}\right|, \tag{4}$$

where v is the azimuthal velocity, r is the radius, ρ is the density, f is the Coriolis parameter, and p is the pressure. The Coriolis term on the left causes acceleration toward the ring center and balances the centripetal acceleration and the pressure gradient force on the right. The pressure gradient arises due to the elevated sea surface height of the WCR. In a WCR with $r \approx 100$ km and $v \approx 1$ m s^{-1}, the Coriolis and pressure gradient terms are on the order of 10^{-4} m s^{-2} and the centripetal acceleration term $|v^2/r|$ is about 1 order of magnitude smaller. In fact, the slightly simpler geostrophic balance, which neglects the $|v^2/r|$ term, is a fairly good approximation in this case, giving

$$|fv| = \left|\frac{1}{\rho}\frac{\partial p}{\partial r}\right|. \tag{5}$$

Given the geostrophic balance of Eq. 5, any process which slows the azimuthal velocity in the WCR will result in a pressure-driven radial outflow. Such a decrease in velocity is typically caused by viscous effects, including interaction with the atmosphere or the surrounding fluid. Although it is possible that an anticyclonic wind (or a wind field with a sufficiently negative curl) aligned with a WCR could act to increase the WCR current speeds, this is not typical. WCRs are observed to slowly decrease in intensity as they drift across the Gulf. Any decrease in the azimuthal current speed disrupts the balance of Eqs. 4 and 5 and (as long as $|v^2/r|$ is sufficiently small) leads to the pressure gradient force dominating. In the WCR, this results in near-surface radial outflow and is more fully investigated in Flierl and Mied (1985). This result is well known in atmospheric flows and is most notable in the inflow region of a hurricane.

By carefully tracking the drifter particles shown in Fig. 3, it is possible to directly estimate the deformation caused by the flow. Since the box is quickly deformed from its

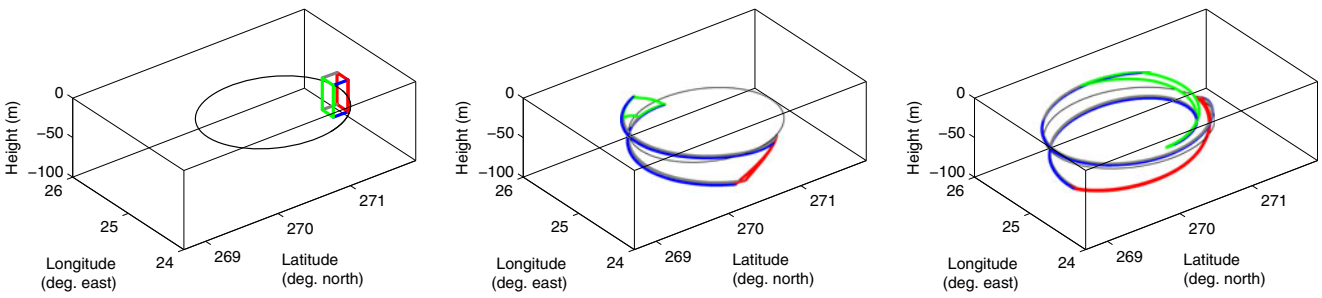

Fig. 3 A box of drifters placed in the checkerboard LCS region of a WCR. The drifter positions are shown at times of 0, 12.5, and 25 days. The *black circle* shows the approximate position of the center of the checkerboard region surrounding the warm-core ring

initial configuration, care must be used in such computations. Here, we focus on the circumferential length of the box and the radial thickness. The circumferential length is computed as the mean length of the elongating edges of the box, computed by integrating along each of these edges. The radial thickness is computed as the average of the distance between points on the longest two edges of the upper and lower faces of the box. To ensure accuracy, only the middle half of these edges is used. The results of this process are plotted in Fig. 4. The length of the box increases approximately linearly for the entire 25 day time period at a rate of approximately 17.2 km day^{-1}. The radial thickness decreases approximately exponentially over this same period, reaching a thickness of about 1.6 km after 25 days.

The flow deformation revealed in this analysis gives two additional insights. First, the observed stretching occurs over a relatively large region of space (an initially 21 km × 21 km × 50 m box) and time (25 days). The passive drifters that begin in this checkerboard LCS region remain in the checkerboard LCS region for the entire 25-day time period investigated and experience consistent deformation in both the circumferential length and radial thickness directions as shown in Fig. 4. Secondly, the velocity field appears to consist of three main components in the checkerboard region: (1) a large and sheared velocity component in the azimuthal direction, (2) a small radial outflow near the surface, and (3) a small compression and upward motion in the vertical direction which must be balanced by expansion in the radial direction for conservation of volume. We note that aspects (2) and (3) do not necessarily imply that the WCR is expanding in radius since the details of these effects at the outer edges of the WCR are not studied here. In fact, WCRs are not observed to grow in radius throughout their existence which could be explained by a number of effects including a small amount of fluid "leaking" from the WCR at the edges and a small downflow near the outer margins of the WCR leading to a slow recirculation rather than outward expansion. Finally, we note that these observations align very well with the velocity structure of WCRs reported by Flierl and Mied (1985), further verifying that the ECCO2 model is accurately capturing the WCR structure.

4 Checkerboard LCS model

As discussed in the previous section, the checkerboard LCS pattern is a new and prominent feature observed in this WCR. This pattern only appears in the mixed layer and there is a sharp transition at the bottom of the mixed layer from the transversely intersecting LCS above to the parallel LCS below. We attribute this sudden change to the greatly reduced radial and vertical flow components below the mixed layer. In the mixed layer, boundary interactions and wind forcing cause unique flow characteristics which can generate the checkerboard LCS pattern. Specifically, wind forcing influences the near-surface velocity field through frictional effects and disrupts the cyclo-geostrophic balance of the WCR. This leads to a pressure gradient-driven radial flow component due to the elevated sea surface height of the WCR. This radial outflow component decreases quickly with depth, leading to relatively large values of shear rate in the radial flow. Combined with the shear in the much larger azimuthal velocity component, these two shear components in different planes acts to create stretching that depends on the direction of time integration. When a small perturbation is added, this generates the checkerboard LCS pattern seen in the WCR. A small amount of compression in the vertical direction was also observed, but it is omitted from the model since the resulting stretching was much smaller than that due to shear effects.

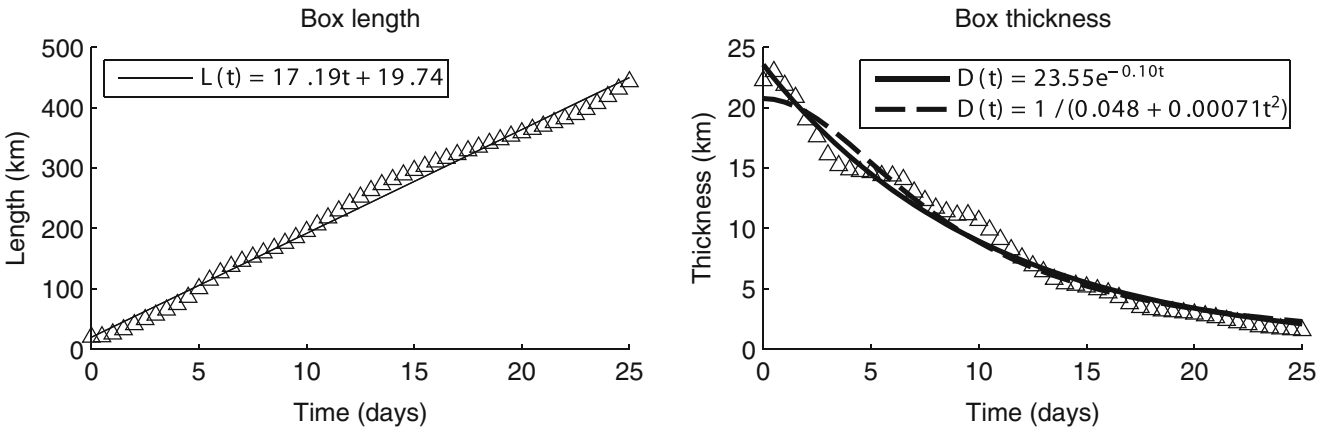

Fig. 4 The deformed circumferential length and radial thickness of the drifter box shown in Fig. 3. The length grows linearly at a rate of about 17.2 km day^{-1} while the thickness decays approximately exponentially. As shown, a fit of $D(t) = 1/(c_1 + c_2 t^{c_3})$ was also tried for the thickness, but the exponential function provides a better fit. A least squares best fit was used to determine the regression curves

The model we use is a simple, non-time-dependent velocity field given by

$$\begin{aligned}\dot{x} &= \dot{\gamma}_1 z,\\ \dot{y} &= \dot{\gamma}_2 x\left[1+\varepsilon\sin\left(\frac{2\pi}{\lambda}y\right)\right],\\ \dot{z} &= 0,\end{aligned} \tag{6}$$

where $\dot{\gamma}_1$ and $\dot{\gamma}_2$ are shear rates, ε is a small perturbation magnitude, and λ is the perturbation wavelength. Although this flow is given in Cartesian coordinates, x, y, and z are analogous to the radial, azimuthal, and vertical directions in the WCR. The y dependence is periodic just as the WCR is periodic in the azimuthal direction. The periodic perturbation is associated with deviations from axisymmetry in the WCR. To more closely match the velocity magnitudes seen in the WCR, constants could be added to the velocity components in Eq. 6. However, constant terms have no affect on the resulting FTLE values or LCS so they are omitted here for simplicity.

To understand why this flow creates the checkerboard pattern in the LCS, we consider the affect of each flow component separately. This is shown schematically in Fig. 5. Starting from an initially square domain in the x-z plane, representing the region for which the LCS will be computed (similar to the view shown in Fig. 6), the $\dot{x}$ component shears the square into a *rhombus* in opposite directions depending on whether the forward or backward flow map is

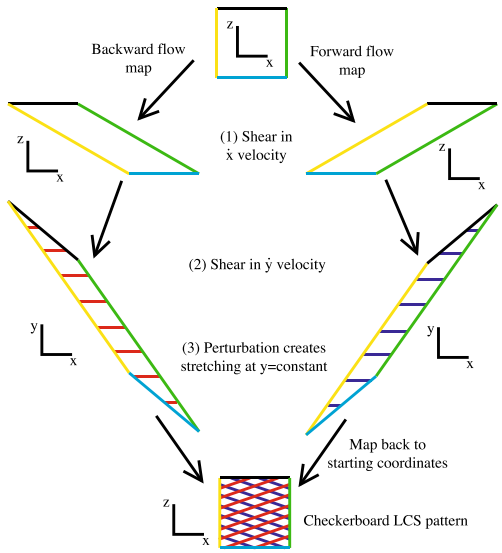

Fig. 5 The stretching behavior resulting from Eq. 6. An initial square at constant y is stretched into a rhombus in different directions by the forward or backward flow map based on the shear in the $\dot{x}$ flow component. This is analogous to shear in the radial outflow of the WCR. Then, looking down the z-axis (a top view), the $\dot{y}$ component shears the rhombus in the y direction. This is analogous to shear in the azimuthal velocity of the WCR. Finally, the perturbation creates localized stretching and LCS at locations that have been mapped to $y(T)$ =constant for an integration time T

considered. The $\dot{y}$ component shears the rhombus out of the x-z plane in the y direction. Perturbations to the flow then act at positions that have been mapped to $y(T)$ =constant, generating larger stretching at these locations and thereby creating LCS. The perturbation is crucial to the generation of the checkerboard LCS. Without it, the stretching would be constant in space and no LCS would be created. These LCS are aligned as shown in Fig. 5. The LCS actually appear in the original coordinates so the final positions where the stretching occurs are mapped back to the original coordinates (inverting the flow map), and create transversely intersecting forward and backward LCS as shown at the bottom of Fig. 5.

The velocity field of Eq. 6 is simple enough to be integrated analytically, but the full solution for $y(t)$ is sufficiently complex that it is most instructive to examine the flow for $\varepsilon = 0$ and then consider the effect of the perturbation. If $\epsilon = 0$, the flow map from $t = 0$ to $t = T$ is

$$\begin{aligned}x(T) &= x_0 + \dot{\gamma}_1 z_0 T\\ y(T) &= y_0 + \dot{\gamma}_2\left(x_0 T + \frac{1}{2}\dot{\gamma}_1 z_0 T^2\right)\\ z(T) &= z_0.\end{aligned} \tag{7}$$

Thus, material which is mapped to $y(T)$ = constant and therefore acted on uniformly by the perturbations originates on the plane defined by

$$y(T) = y_0 + \dot{\gamma}_2\left(x_0 T + \frac{1}{2}\dot{\gamma}_1 z_0 T^2\right) \tag{8}$$

where (x_0, y_0, z_0) are the starting coordinates. The perturbation creates compression and expansion in $y(T)$ at a wavelength of λ. Thus, we expect the resulting LCS to spaced at intervals of

$$\Delta x = \frac{\lambda}{\dot{\gamma}_2 T}, \quad \Delta y = \lambda, \quad \Delta z = \frac{2\lambda}{\dot{\gamma}_1\dot{\gamma}_2 T^2}, \tag{9}$$

and a slope in x-z plane of

$$\frac{\Delta z}{\Delta x} = \frac{2}{\dot{\gamma}_1 T}. \tag{10}$$

These results are valid for $\varepsilon \ll 1$. A more detail analysis of the full solution of Eqs. 6 reveals that larger values of ε increase the spacing between the LCS, but do not change the slope.

To compare the model velocity field to the checkerboard LCS seen in the WCR from the ECCO2 simulation, we must first estimate the parameters $\dot{\gamma}_1$, $\dot{\gamma}_2$, and λ in the WCR. $\dot{\gamma}_1$ corresponds to the shear rate of the radial velocity component with respect to the vertical direction. An examination

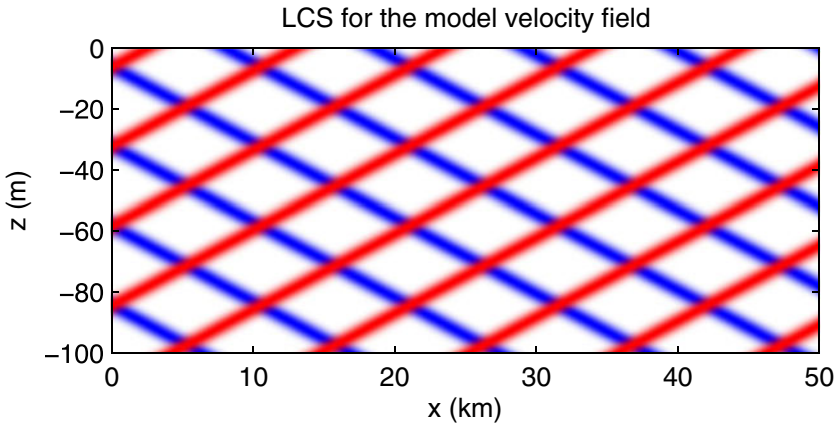

Fig. 6 The LCS resulting from Eq. 6. The LCS show a checkerboard pattern which is similar to the that seen in the WCR. The *red curves* are attracting LCS and the *blue curves* are repelling LCS

of the azimuthally averaged WCR shows that the radial outflow component has a maximum near the surface of about 2.5×10^{-2} m s^{-1} and decreases to zero at a depth of about 75 m so $\dot{\gamma}_1 \approx 3.33 \times 10^{-4}$ s^{-1}. $\dot{\gamma}_2$ corresponds to the shear rate of the azimuthal velocity with respect to the radius in the checkerboard region. In the same way, we find that $\dot{\gamma}_2 \approx 1.15 \times 10^{-5}$ s^{-1} in the checkerboard region. Despite the fact that the radial flow velocity in the WCR is much smaller than the azimuthal component, $\dot{\gamma}_1$ is an order of magnitude larger than $\dot{\gamma}_2$ due to the smaller length scales in the vertical direction. For this reason, the shear in the WCR radial outflow is a critical component for generating the checkerboard LCS pattern.

Finally, we determine the parameters of the model associated with the sinusoidal perturbation. The value of ε does not significantly affect the resulting LCS. We use $\varepsilon = 0.01$, corresponding to a 1 % perturbation of the azimuthal velocity. An examination of the WCR shape reveals that it is slightly elliptical. This is common in WCRs (Cushman-Roisin et al. 1985) and generates a perturbation wavelength of 1/2 the WCR circumference. The circumference of the checkerboard region is about 5.9×10^5 m, giving a value of $\lambda = 2.95 \times 10^5$ m. Computing the LCS in this model with the same integration time that was used for the WCR ($T = \pm 4$ weeks) results in the checkerboard LCS pattern shown in Fig. 6.

To directly compare the checkerboard LCS resulting from the model and the WCR, we examine two metrics: the spacing between the LCS and the slope of the LCS. For the WCR, the LCS have a slope of around 2–3 m km^{-1}, a horizontal spacing of about 8–15 km, and a vertical spacing of 20–40 m depending on precisely where these measurements are made. For the model velocity field of Eq. 6, the LCS have a slope of 2.5 m km^{-1}, a horizontal spacing of 10.6 km, and a vertical spacing of 26.6 m. These results all lie within the range of values measured in the simulated WCR and show very good agreement between the model and the checkerboard region in the WCR.

5 Conclusions

A LCS analysis of a numerically simulated WCR in the Gulf of Mexico has revealed some previously unobserved transport structures. The WCR studied here is present in the ECCO2 global ocean simulation which has proven useful in other studies for investigating ocean eddy behavior. In the WCR, the eddy core is surrounded by a series of "checkerboard" LCS in the mixed layer which form a cross-hatched pattern of transversely intersecting LCS when viewed in the *r*-*z* plane. Fluid in this region undergoes consistent stretching behavior. As with most ocean flows, there is very little vertical transport in the WCR and a box of passive drifter particles placed in the checkerboard region is elongated in the circumferential direction, becoming wrapped around the WCR, while becoming thinner in the radial direction. Such uniform stretching behavior does not admit transport across the checkerboard LCS region, contributing to the long life of WCRs.

A detailed investigation of the Lagrangian stretching behavior in the checkerboard region gives rise to an analytical model which produces similar LCS. The most important parameters of the model are the vertical shear rate of the radial velocity component, the horizontal shear rate of the azimuthal velocity, and the principle wavelength of perturbations representing deviations from axisymmetry. These parameters were estimated directly from the numerically simulated WCR velocity field and used to compute the LCS generated by the model. The LCS produced by this analytical model show very good agreement with those seen in the WCR. Transversely intersecting LCS are produced by the model with slopes and spacings that match those seen in the WCR.

It is important to note that although the velocity field in the simulated WCR is largely two dimensional, the length scales in the vertical direction are much smaller than the horizontal. For this reason, gradients in the vertical direction can be of the same order or larger than those in the horizontal. The analytical model used to produce the

checkerboard LCS here relies on three-dimensional stretching behavior which cannot occur in a two-dimensional domain. Even though the vertical motion is ignored, the vertical shear is critically important. Additionally, the small radial outflow near the surface of the WCR is absolutely critical in producing the transversely intersecting LCS pattern seen here. This radial flow is thought to occur primarily because frictional effects in the mixed layer disrupt the cyclo-geostrophic balance of the WCR and enable a pressure-driven radial outflow. Below the mixed layer, there is essentially no radial flow component and therefore the character of the LCS changes to include only parallel LCS.

The checkerboard LCS seen in this study have been shown to be associated with the shear present in this region of the simulated WCR. In WCRs and other well developed mesoscale ocean eddies, flow tends to be well ordered and laminar and the lack of strong updrafts and overturning flow in WCRs limits the available mechanisms for mixing and homogenization. The presence of the checkerboard LCS reveals one region in the WCR where shear greatly affects the Lagrangian dynamics of fluid motion. A study of drifters placed in this region revealed that a large box-shaped domain is quickly stretched into a long, thin filament around the ring circumference. Small-scale mixing caused by breaking waves, wind gusts, biological interactions, and small-scale turbulence is always present in the ocean and the stretching and shearing in the checkerboard region creates opportunities for mixing and homogenization within the WCR on small scales while minimizing fluid exchange with the surrounding ocean.

The checkerboard LCS pattern that is seen in the simulated WCR studied here suggests several new directions for further study. Firstly, the radial outflow observed near the surface of the WCR is critically important to the generation of the checkerboard LCS pattern. There is good reason to expect this behavior due to frictional effects enabling pressure gradient-driven flow, but the existing literature in this area is limited. Additional ocean studies or high-fidelity numerical models investigating this effect may be quite informative. Additionally, we have focused on a single WCR. It is possible that other WCRs in the ECCO2 simulation or the real world may not meet all the criteria to create the checkerboard LCS. The prevalence of this pattern is currently unknown. Finally, the large fluid shearing and corresponding azimuthal homogenization within the checkerboard region likely has affects on biological systems. It is known that warm-core rings influence phytoplankton blooms (Franks et al. 1986; Biggs 1992) and fish distributions (Olson and Backus 1985) in the ocean. The advective transport in this region will impact the distribution of nutrients, pollutants, temperature, salt, oxygen, etc. within and around the WCR. It would be particularly interesting to investigate the biological effects of the checkerboard region through simulation and observation. The analytical model of Section 4 provides a potential starting point for simplified simulations of the checkerboard region that include biological systems and nutrient distribution.

Acknowledgments The authors gratefully acknowledge the support of the Office of Naval Research in conducting this work.

References

Beron-Vera F, Olascoaga M, Goni G (2008) Oceanic mesoscale eddies as revealed by Lagrangian coherent structures. Geophys Res Lett 35(12):L12603

Biggs D (1992) Nutrients, plankton, and productivity in a warm-core ring in the western Gulf of Mexico. J Geophys Res: Oceans 97(C2):2143–2154

Cardwell B, Mohseni K (2008) Vortex shedding over two-dimensional airfoil: where do the particles come from? AIAA J 46(3):545–547

Chen R (2013) Energy pathways and structures of oceanic eddies from the ecco2 state estimate and simplified models. PhD thesis, Massachusetts Institute of Technology

Coulliette C, Wiggins S (2001) Intergyre transport in a wind-driven, quasigeostrophic double gyre: an application of lobe dynamics. Nonlinear Process Geophys 8(1/2):69–94

Coulliette C, Lekien F, Haller G, Paduan J, Marsden J (2007) Optimal pollution mitigation in Monterey Bay based on coastal radar data and nonlinear dynamics. Environ Sci Technol 41(18):6562–6572

Cushman-Roisin B, Heil WH, Nof D (1985) Oscillations and rotations of elliptical warm-core rings. J Geophys Res: Oceans (1978–2012) 90(C6):11756–11764

Dellnitz M, Grubits K, Marsden JE, Padberg K, Thiere B (2005) Set-oriented computation of transport rates in 3-degree of freedom systems: the Rydberg atom in crossed fields. Regul Chaotic Dyn 10(2):173–192

Elliott B (1979) Anticyclonic rings and the energetics of the circulation of the gulf of mexico. PhD thesis, Texas A&M Univ

Farazmand M, Haller G (2012) Computing Lagrangian coherent structures from variational theory. Chaos 22(1):013128–013128

Flierl GR, Mied RP (1985) Frictionally induced circulations and spin down of a warm-core ring. J Geophys Res: Oceans (1978–2012) 90(C5):8917–8927

Franks PJ, Wroblewski J, Flierl GR (1986) Prediction of phytoplankton growth in response to the frictional decay of a warm-core ring. J Geophys Res 91(C6):7603–7610

Froyland G, Padberg K (2009) Almost-invariant sets and invariant manifolds—connecting probabilistic and geometric descriptions of coherent structures in flows. Phys D 238:1507–1523

Fu LL (2009) Pattern and velocity of propagation of the global ocean eddy variability. J Geophys Res 114(C11):C11017

Green M, Rowley C, Haller G (2007) Detection of Lagrangian coherent structures in three-dimensional turbulence. J Fluid Mech 572(1):111–120

Haller G (2002) Lagrangian coherent structures from approximate velocity data. Phys Fluids 14(6):1851–1861

Haller G (2004) Exact theory of unsteady separation for two-dimensional flows. J Fluid Mech 512:257–311

Haller G (2011) A variational theory of hyperbolic Lagrangian coherent structures. Phys D 240:574–598

Haller G, Yuan G (2000) Lagrangian coherent structures and mixing in two dimensional turbulence. Phys D 147:352–370

Hong X, Chang SW, Raman S, Shay LK, Hodur R (2000) The interaction between Hurricane Opal (1995) and a warm core ring in the Gulf of Mexico. Mon Weather Rev 128(5):1347–1365

Huntley H, Lipphardt B, Kirwan A, Hogan P (2013) Surface drift predictions of the Deepwater Horizon spill: the Lagrangian perspective. In: Liu Y, Macfadyen A, Ji ZG, Weisberg RH (eds) Monitoring and modeling the deepwater horizon oil spill: a record-breaking enterprise. American Geophysical Union, Washington, D.C., pp 179–195

Hurlburt H, Thompson J (1980) A numerical study of loop current intrusions and eddy shedding. J Phys Oceanogr 10(10):1611–1651

Ide K, Small D, Wiggins S (2002) Distinguished hyperbolic trajectories in time-dependent fluid flows: analytical and computational approach for velocity fields defined as data sets. Nonlinear Process Geophys 9:237–263

Joyce T, Kennelly M (1985) Upper-ocean velocity structure of Gulf Stream warm-core ring 82B. J Geophys Res: Oceans (1978–2012) 90(C5):8839–8844

Kanamitsu M, Ebisuzaki W, Woollen J, Yang SK, Hnilo J, Fiorino M, Potter G (2002) NCEP-DOE AMIP-II reanalysis (R-2). Bull Am Meteorol Soc 83(11):1631–1643

Kishi MJ (1994) Prediction of phytoplankton growth in a warm-core ring using three dimensional ecosystem model. J Oceanogr 50(5):489–498. doi:10.1007/BF02235419

Lekien F, Ross S (2010) The computation of finite-time Lyapunov exponents on unstructured meshes and for non-Euclidean manifolds. Chaos 20:017504. doi:10.1063/1.3278516

Lewis JK, Kirwan A, Forristall GZ (1989) Evolution of a warm-core ring in the Gulf of Mexico: Lagrangian observations. J Geophys Res: Oceans 94(C6):8163–8178

Lipinski D, Mohseni K (2009) A numerical investigation of flow structures and fluid transport with applications to feeding for the hydromedusae Aequorea victoria and Sarsia tubulosa. J Exp Biol 212:2436–2447

Lipinski D, Mohseni K (2012) A 3D fast algorithm for computing Lagrangian coherent structures via ridge tracking. arXiv preprint arXiv:1202.5236

Madrid J, Mancho A (2009) Distinguished trajectories in time dependent vector fields. Chaos 19:013111 (18 pp)

Marshall J, Adcroft A, Hill C, Perelman L, Heisey C (1997) A finite-volume, incompressible Navier Stokes model for studies of the ocean on parallel computers. J Geophys Res: Oceans (1978–2012) 102(C3):5753–5766

Menemenlis D, Campin JM, Heimbach P, Hill C, Lee T, Nguyen A, Schodlok M, Zhang H (2008) ECCO2: high resolution global ocean and sea ice data synthesis. Mercator Ocean Q Newsl 31: 13–21

Mezić I, Loire S, Fonoberov VA, Hogan P (2010) A new mixing diagnostic and Gulf oil spill movement. Science 330(6003):486–489

Oey L (2008) Loop current and deep eddies. J Phys Oceanogr 38(7):1426–1449

Olascoaga M, Haller G (2012) Forecasting sudden changes in environmental pollution patterns. Proc Natl Acad Sci 109:4738–4743. doi:10.1073/pnas.1118574109

Olson DB, Backus RH (1985) The concentrating of organisms at fronts: a cold-water fish and a warm-core gulf stream ring. J Mar Res 43:113–137

Olson D, Schmitt R, Kennelly M, Joyce T (1985) A two-layer diagnostic model of the long-term physical evolution of warm-core ring 82B. J Geophys Res: Oceans (1978–2012) 90(C5):8813–8822

Peng J, Dabiri J (2009) Transport of inertial particles by Lagrangian coherent structures: application to predator-prey interaction in jellyfish feeding. J Fluid Mech 623:75–84. doi:10.1017/S0022112008005089

Scharroo R, Smith WH, Lillibridge JL (2005) Satellite altimetry and the intensification of Hurricane Katrina. Eos, Trans Am Geophys Union 86(40):366

Shadden S, Lekien F, Marsden J (2005) Definition and properties of Lagrangian coherent structures from finite time Lyapunov exponents in two-dimensional aperiodic flows. Phys D 212:271–304

Shay LK, Goni GJ, Black PG (2000) Effects of a warm oceanic feature on Hurricane Opal. Mon Weather Rev 128(5):1366–1383

Sturges W, Leben R (2000) Frequency of ring separations from the loop current in the Gulf of Mexico: a revised estimate. J Phys Oceanogr 30(7):1814–1819

Sulman MH, Huntley HS, Lipphardt B Jr, Kirwan A Jr (2013) Leaving flatland: diagnostics for Lagrangian coherent structures in three-dimensional flows. Phys D Nonlinear Phenom 258: 77–92

Volkov DL, Fu LL (2008) The role of vorticity fluxes in the dynamics of the Zapiola Anticyclone. J Geophys Res: Oceans (1978–2012) 113(C11). doi:10.1029/2008JC004841

Volkov DL, Lee T, Fu LL (2008) Eddy-induced meridional heat transport in the ocean. Geophys Res Lett 35(20). doi:10.1029/2008GL035490